A Low-Power Analog Integrated Gaussian-based Neural Network Classifier with Application to Hepatitis Disease Recognition

Vassilis Alimisis, Nikolaos P. Eleftheriou and Paul P. Sotiriadis

Department of Electrical and Computer Engineering
National Technical University of Athens, Greece
E-mail: alimisisv@gmail.com, eleftheriou_nikos@hotmail.com , pps@ieee.org

2023 International Conference on Microelectronics (ICM) | 979-8-3503-8082-8/23/$31.00 ©2023 IEEE | DOI: 10.1109/ICM60448.2023.10378941

***Abstract*—Hepatitis is a medical condition characterized by inflammation of the liver. It can be triggered by various factors, including viral infections, excessive alcohol consumption, specific medications, or autoimmune disorders. Recognizing hepatitis early is crucial in reducing its symptoms, as it allows for timely treatment. In this study, a low-power ($4.31\mu W$) and low-voltage (0.6V) analog artificial neural network classifier is introduced, utilizing a Gaussian-based activation function. The architecture comprises a hidden layer: with a Gaussian activation function circuit and $\tanh$ approximation, an output layer with a softmax function circuit, and an argmax operator. A comparative analysis is performed to evaluate the performance of this methodology against commonly used analog classifiers. To conduct this assessment, a real-world hepatitis dataset is employed. The models are trained and results processed using the Python programming language. The hardware design and result processing are executed using Cadence IC Suite, utilizing the TSMC 90nm CMOS process technology, demonstrating the practical applicability and effectiveness of this methodology.**

***Index Terms*—Artificial Neural Network, analog VLSI implementation, hepatitis classification, low-power design**

I. Introduction

Machine Learning (ML) and Artificial Intelligence (AI) have revolutionized bioengineering and healthcare, ushering in a new era of personalized, data-driven medical practices [1]. These technologies enable in-depth analysis of vast sets of biological and clinical data, offering unprecedented insights into disease mechanisms, treatment responses, and patient outlooks [1]. In bioengineering, ML algorithms are utilized to craft and enhance tailored medical devices, prosthetics, and implants [2]. Additionally, AI-powered image analysis has greatly enhanced diagnostic precision in medical imaging, swiftly detecting abnormalities and tumors.

Regarding healthcare, prognostic models utilize patient data to predict the trajectory of diseases, enabling proactive interventions [2]. Additionally, natural language processing facilitates the extraction of invaluable information from clinical records and academic literature, expediting medical research and knowledge acquisition [3]. The integration of ML and AI in bioengineering and healthcare not only elevates the standard of patient care but also lays the foundation for pioneering innovations with the potential to revolutionize the future of medicine [4].

The hardware implementation of ML and AI in bioengineering is a pivotal frontier in modern healthcare tech [1]. Specialized systems process vast datasets, enabling real-time decision-making in medical applications. Customized circuits and accelerators handle complex ML algorithms, optimizing tasks like image recognition and predictive modeling. Neuromorphic computing mimics the human brain's neural networks, offering parallel processing for tasks like pattern recognition [5]. These hardware advances boost the speed and efficiency of ML and AI in bioengineering, with potential to revolutionize patient care and medical research.

Analog computing is rapidly advancing in the field of bioengineering for ML and AI applications [6]. This approach utilizes continuous signals and physical phenomena to process complex biological data, mirroring the continuous nature of biological systems. This is particularly beneficial for real-time responses in bioengineering, where intricate physiological processes are common. Specialized analog circuits mimic neuron behavior, efficiently processing neural network models. Analog computing excels in tasks like signal processing and pattern recognition, proving invaluable in medical imaging and biosignal analysis [7]. Its precision and speed are poised to drive significant progress in personalized medicine, prosthetic design, and bioinformatics, leading to more effective healthcare solutions and improved patient outcomes.

Motivated by the low-power and area efficiency requirements of smart sensors for biomedical applications [8], [9], this work proposes a low-power ($4.31\mu W$) and low-voltage (0.6V) analog artificial neural network (ANN) classifier, utilizing a Gaussian-based activation function. The implemented classifier is a promising approach, appropriate for battery dependent smart sensor classification systems, since it achieves 96.42% accuracy. It is designed and verified on a real-world hepatitis disease recognition dataset [10]. The post-layout simulation results, performed in a TSMC 90nm CMOS process and simulated using Cadence IC Suite, confirm the accuracy of the proposed implementation through comparison with a software-based approach and analog related classifiers.

The remainder of this paper is organized as follows. Section II refers to the background; explains the ANN approach and the hepatitis disease. In Section III the proposed architecture and the basic building blocks of the proposed classifier are thoroughly explained. In Section IV, the proposed classifier's performance is validated using a real-world dataset for hepatitis disease recognition and is contrasted with the software-based implementation. Section V conducts a comparative study with analog classifiers in the field. Concluding remarks are presented in Section VI.

II. Background

A. Artificial Neural Network Model

An ANN, inspired by the human brain's neural network system, is a potent computational model [11]. It comprises layers of interconnected neurons. Each neuron processes and transmits information, with the input layer receiving data. This data is weighted and processed through hidden layers for complex computations. The output layer produces the final prediction or classification. Through backpropagation during training, the network adjusts its internal parameters, minimizing the error between predicted and actual outcomes. This capability allows ANNs to discern intricate patterns in data, making them invaluable in tasks such as image recognition, speech processing, and predictive modeling. ANNs have transformed various fields, showcasing their adaptability and potential in solving complex problems.

ANNs can be mathematically represented at different levels of abstraction. Here are some of the fundamental equations [11] that describe the workings of a simple feedforward neural network; neuron input (weighted sum), activation function and feedforward process. The input to a neuron in a feedforward network is calculated as the weighted sum of its inputs, followed by the addition of a bias term and the application of an activation function. This can be represented as:

$$z_j = \sum_{i=1}^{n} w_{ij} x_i + b_j. \tag{1}$$

Where:

- z_j is the weighted sum for neuron j.
- w_{ij} represents the weight connecting neuron i to neuron j.
- x_i is the output of neuron i in the previous layer.
- b_j is the bias term for neuron j.

The output of a neuron is obtained by applying an activation function to the weighted sum. Common activation functions include $sigmoid$, Rectified Linear Unit (ReLU) , $\tanh$, and softmax. For instance, the $sigmoid$ activation function is defined as:

$$a_j = \sigma(z_j) = \frac{1}{1 + e^{-z_j}}. \tag{2}$$

Here, a_j is the output (activation) of neuron and σ represents the $sigmoid$ function. In a feedforward network, the outputs of one layer serve as the inputs to the next. This process continues until the final layer provides the network's output.

$$x_j^{(l+1)} = \sigma(\sum_{i=1}^{n} w_{ij}^{(l)} x_i^{(l)} + b_j^{(l)}). \tag{3}$$

Here, $x_j^{(l)}$ is the output of neuron j in layer l, $w_{ij}^{(l)}$ are the weights connecting neurons between layers l and $l+1$ and $b_j^{(l)}$ is the bias term for neuron j in layer l. These equations form the basis for understanding the computations that occur within a feedforward ANN.

B. Hepatitis Disease

Hepatitis is a widespread medical condition characterized by inflammation of the liver [12]. It can be caused by various factors, with viral infections being the most common culprits. Hepatitis viruses are categorized from A to E, each with distinct transmission methods and potential outcomes. For instance, Hepatitis A and E are typically contracted through contaminated food or water, while Hepatitis B, C, and D are primarily transmitted through contact with infected blood or other bodily fluids. Chronic forms of Hepatitis, particularly B and C, can lead to serious liver complications over time, such as cirrhosis and even liver cancer if left untreated. It's imperative to prioritize prevention through vaccination, safe hygiene practices, and public health education to mitigate the spread of hepatitis.

III. Proposed Architecture

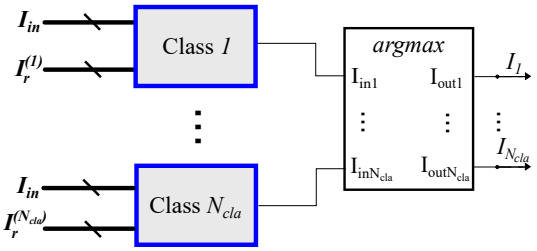

Fig. 1: The high level architecture of the proposed ANN classifier which combines N_{cla}, N_d input features. It consists of N_{cla} class cells and $argmax$ operator with N_{cla} inputs.

In this section, the proposed analog implementation of the ANN is analysed. The introduced architecture is adaptable, capable of handling different quantities of classes and input dimensions. The structure of the suggested classifier, depicted in Fig. 1, is tailored for a classification task with N_{cla} classes and N_d input dimensions. The number of layers in each class is a hyper-parameter, typically determined through exploratory data analysis. For simplicity, it consists of 1 hidden layer in each class. The proposed architecture's k-th ($k \in \{1, ..., N_{cla}\}$) class comprises a hidden layer: with a Gaussian activation function circuit (GHL) and $\tanh$ approximation (THL), an output layer with a softmax function circuit, and a Voltage-to-Current (V/I) converter, as shown in Fig. 2.

Firstly, the inputs are sent to a hidden layer which performs a nonlinear Gaussian function as activation function, on the

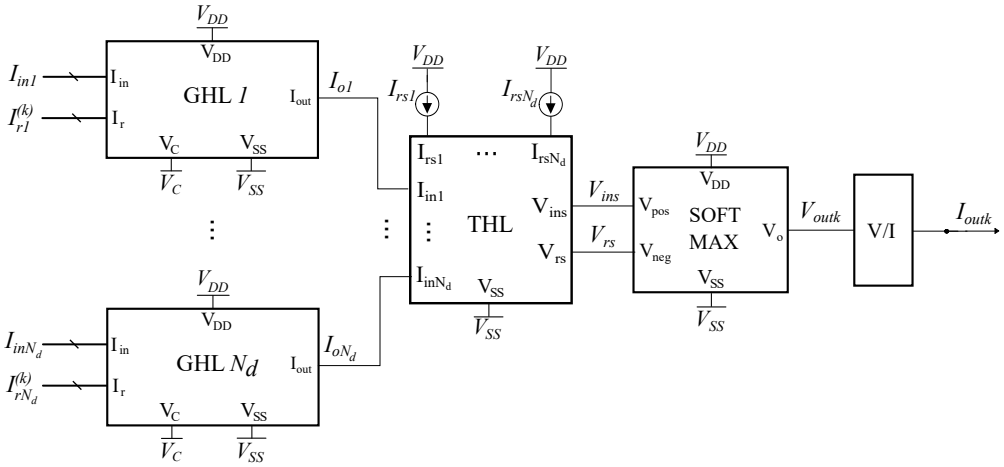

Fig. 2: The proposed architecture's k-th ($k \in \{1, ..., N_{cla}\}$) class comprises a hidden layer: with a Gaussian activation function circuit (GHL) and $\tanh$ approximation (THL), an output layer with a softmax function circuit, and a Voltage-to-Current (V/I) converter.

weighted sum of all inputs. The input currents are adjusted to restrict the input range for the hidden layer between -0.3V and 0.1V, ensuring that the input transistors in the hidden layer never enter the linear region. For the implementation of the Gaussian function as activation function, a current-mode Gaussian function circuit [13] is employed. It is shown in Fig. 3 and the dimensions of the transistors are summarized in Table I. In particular, the I_{in} is the input current and the current parameter I_r, the voltage parameter V_c, and the bias current I_{bias} regulate the mean value, variance, and amplitude, respectively.

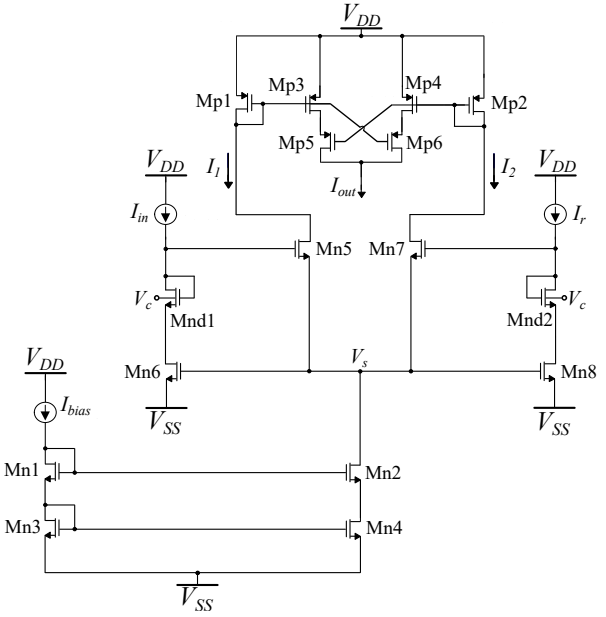

Fig. 3: The current-mode Gaussian activation function circuit.

The second component in the hidden layer is a straightforward NMOS cascode current mirror with a PMOS diode load, which is shown in Fig. 4. Since all transistors operate in the sub-threshold region, this unit imparts an approximately $\tanh$ behavior to the output current of the Gaussian function circuit. This method significantly trims down hardware expenses when compared to conventional circuit implementations of these activation functions. In the proposed ANN classifier, weight vectors are realized by adjusting the bias current I_{bias} of the preceding Gaussian function circuit block. For each class, a set of N_d basic NMOS cascode current mirrors (CCMs) with a PMOS diode load is employed. These circuits are linked to the output of the respective Gaussian function circuits, receiving an input current I_{ok} ($k \in \{1, ..., N_{cla}\}$). A second set of N_d basic NMOS CCMs with a PMOS diode load is put into operation and biased with a current I_{rsk} ($k \in \{1, ..., N_{cla}\}$). The current I_{rsk} serves as a parameter current, supplied during the classifier's training.

TABLE I: MOS Transistors' Dimensions (Fig. 3).

Block	**W/L** (μm/μm)	**Current Correlator**	**W/L** (μm/μm)
M_{n1}-M_{n6}	0.8/1.6	M_{p1}-M_{p2}	0.8/1.6
M_{n7}, M_{n9}	0.4/1.6	M_{p3}-M_{p6}	0.4/1.6
M_{n8}, M_{n10}	1.6/1.6	-	-

Both sets of NMOS cascode current mirrors generate output voltages, namely V_{ins} and V_{rs}, as depicted in Fig. 4. These voltages are subsequently fed into the output layer. The output neuron is implemented as a pseudo-differential current mirror, carrying out the softmax operation on the weighted sum of the outputs from the hidden layer, which is shown in Fig. 4 (middle block). Following this, the output voltage (V_o) from each softmax block is directed into a V/I converter [14], shown in Fig. 5, which produce the appropriate output current. Then, all the output currents are fed into the argamx operator circuit (determining the winning class).

Moving forward, the ANN is established using an argmax operator circuit, specifically employing a Winner-Take-All (WTA) circuit [15]. In a classification problem featuring N_{cla}

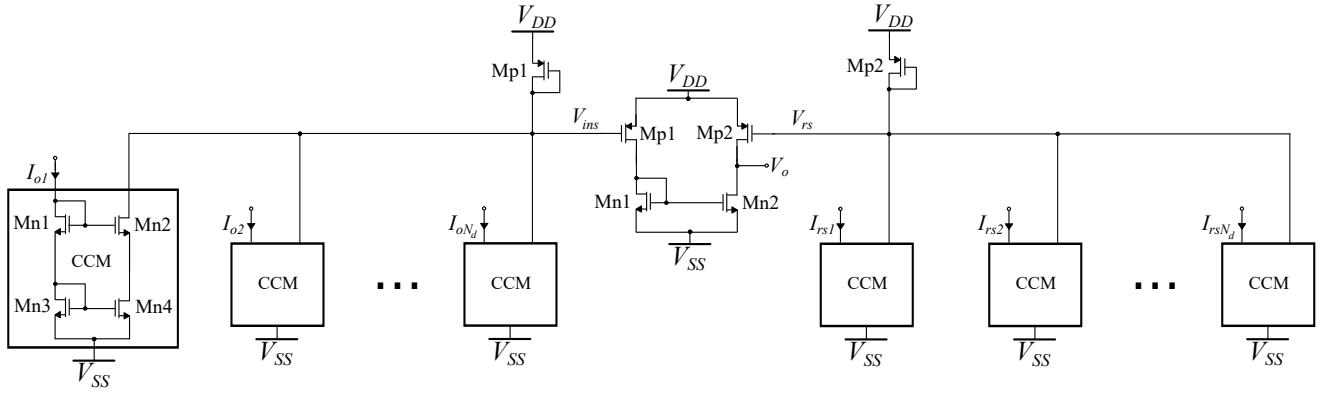

Fig. 4: A set of N_d basic NMOS CCMs with a PMOS diode load linked to the output of the respective Gaussian function circuits (left). A second set of N_d basic NMOS CCMs with a PMOS diode load is put into operation and biased with a current I_{rsk} (right). A pseudo-differential current mirror, carrying out the softmax operation (middle)

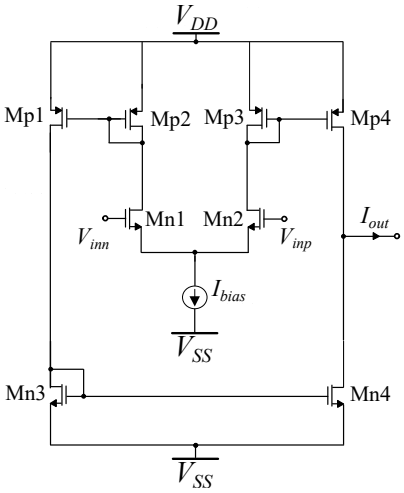

Fig. 5: The implementation of V/I converter.

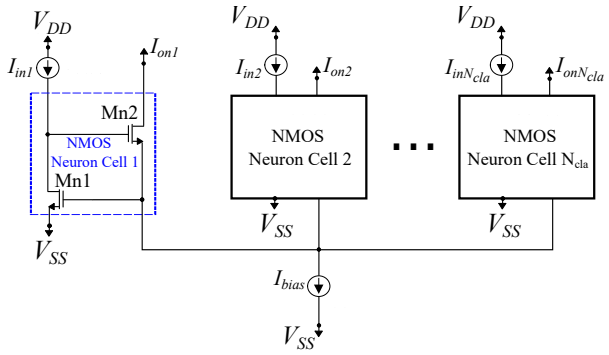

Fig. 6: A N_{cla}-neuron Standard Lazzaro NMOS Winner-Take-All (WTA) circuit.

classes, the standard Lazzaro WTA circuit encompasses N_{cla} neurons. These neurons collectively share a common bias current, as illustrated in Fig. 6. Each neuron within the WTA circuit corresponds to an individual class. The WTA circuit efficiently discerns the class with the highest input current and allocates a non-zero output current to the respective neuron. Concurrently, the remaining neurons receive an output current of zero. Notably, all transistors in the mentioned designs operate in the sub-threshold region, with power supply rails set as $V_{DD} = -V_{SS} = 0.3$V.

IV. Hepatitis Dataset and Simulation Results

In this Section, the proper operation of the proposed classifier is confirmed via a real-world hepatitis disease recognition dataset [10]. It is provided by University of California, Irvine (UCI) Machine Learning Repository. It contains valuable information related to the liver disease, hepatitis, which is a significant global health concern. It encompasses various laboratory test results, and presence of hepatitis B and C viruses. By leveraging it, experts can gain deeper insights into the factors influencing the onset and progression of hepatitis, ultimately contributing to improved diagnostic and treatment strategies for individuals affected by this condition.

The proposed architecture is implemented using the TSMC $90nm$ CMOS process with the aid of the Cadence IC suite. The entire classifier is powered with $V_{DD} = -V_{SS} = 0.3V$. All the simulation results are provided from the implemented layout, which is depicted in Fig. 7 (post-layout simulations). This study addresses a hepatitis disease recognition problem, involving $N_{cla} = 2$ classes and $N_d = 19$ inputs. It's a binary classification task wherein the classifier determines whether a patient is healthy or afflicted with hepatitis, making it a binary classifier. The relevant metrics (attributes) mentioned earlier are directly inputted into the classifier. The system's essential parameters are derived by calculating the mean value, variance, and prior probability for each class.

To comprehensively evaluate the proposed classifier in terms of classification specificity and its performance under varying Process, Voltage, and Temperature (PVT) conditions, two distinct tests are conducted on the layout. To account for experimental variability, the results from 20 different training-test iterations are shown in Fig. 8. The circuit's sensitivity is further confirmed through a Monte Carlo analysis. Specifically,

Fig. 9 illustrates the Monte Carlo Histogram based on N = 100 points, providing further insights into the circuit's robustness and performance characteristics It has a mean value of $\mu_M = 95.98\%$ and a standard deviation of $\sigma_M = 1.37\%$.

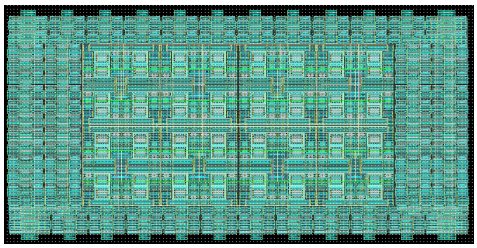

Fig. 7: The layout of the proposed architecture.

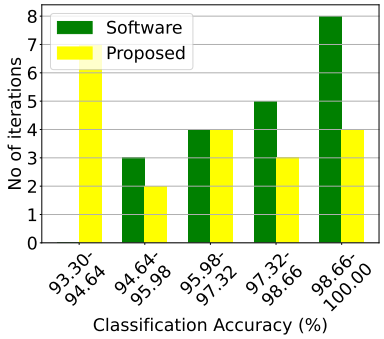

Fig. 8: Classification results of the proposed architecture and the equivalent software model on the hepatitis disease recognition dataset over 20 iterations.

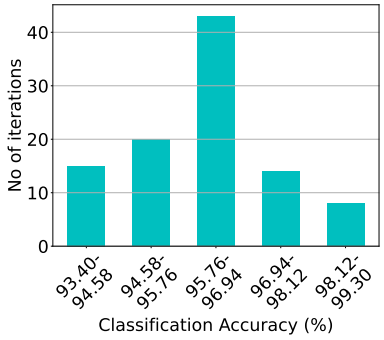

Fig. 9: Post-layout Monte-Carlo simulation results of the proposed architecture on the hepatitis disease recognition dataset with $\mu_M = 95.98\%$ and a standard deviation of $\sigma_M = 1.37\%$

V. Comparison and Discussion

In the realm of current literature, it is evident that a significant portion of analog classifiers is customarily designed to cater to particular applications. This circumstance poses a challenge when attempting to execute an unbiased comparison across varied implementations. Nevertheless, this challenge offers us the opportunity to modify analog classifiers to suit a common application, thereby streamlining a performance evaluation encompassing both machine learning models and alternative methodologies Notably, Table III provides an overview of the performance metrics of our study in conjunction with comparable classifiers like ANN [16], Radial Basis function [17], Multilayer Perceptron (MLP) [18], Long Short-Term Memory (LSTM) [19], K-means [20], Bayesian [13], Gaussian Mixture Model (GMM) [22], Fuzzy [21], Threshold [23], Support Vector Machine (SVM) [24] and centroid-based [25] all within the context of hepatitis disease recognition.

The proposed work presents an intriguing solution as it offers a trade-off between accuracy, power, and energy consumption per classification when compared to related analog classifiers. It's crucial to emphasize that, in this specific application, the design is handling a high input dimensionality. The proposed topology provides a notable advantage by eliminating the need for Principal Component Analysis (PCA), allowing for the utilization of all 19 input dimensions without any loss of information. To attain optimal accuracy, several other topologies need to reduce the dimensions to 12, which represents a notable limitation in previous related works, except from the more complex models [16], [18]–[20]. While the proposed classifier showcases the ability to accurately classify more classes, we select a binary classification scenario for fair comparison. This adjustment enables a more meaningful comparison with binary analog classifiers [21], [23], [24].

In terms of classification accuracy, the proposed architecture surpasses all related classifiers except for MLP [18] and LSTM [19]. These models, while achieving higher accuracy, are more complex and require more power and hardware area (due to having more components). The Threshold classifier achieves the lowest power consumption, albeit at the expense of accuracy and processing speed, owing to its straightforward model design [23]. It's worth emphasizing that in biomedical applications of this nature, rapid processing speed is not a critical requirement, primarily due to their low occurrence frequency. Consequently, in the proposed approach, processing speed is intentionally reduced to enhance accuracy and optimize power consumption performance. Furthermore, it boasts lower energy consumption per classification compared to all classifiers, with the exception of ANN [16], which achieves lower classification accuracy.

VI. Conclusion

In this work, a low power ($4.31\mu W$), low voltage (0.6V) architecture of an analog Gaussian-based ANN classifier for hepatitis disease recognition was proposed. The presented architecture consists of a hidden layer with a Gaussian activation function circuit, an output layer with a softmax function circuit, and an argmax operator. The post-layout simulation results were conducted utilizing the TSMC 90nm CMOS process and were compared with both a software-based implementation and a range of analog classifiers. The realized architecture attains a classification accuracy of 96.42% along with satisfactory sensitivity characteristics. It can act as a fundamental component in diverse wearable biomedical devices, particularly those with stringent power consumption requirements.

TABLE II: Analog classifiers' comparison on the Hepatitis Disease Recognition

	Classifier	Worst accuracy	Mean accuracy	Best accuracy	Power consumption	Processing speed	Energy per classification	No. of Dimensions
This work	ANN	93.30%	96.42%	99.40%	$4.31\mu W$	$1.2M\frac{\text{classifications}}{\text{s}}$	$\frac{3.59\text{ pJ}}{\text{classification}}$	19
[16]	ANN	91.70%	94.78%	97.90%	$3.12\mu W$	$14M\frac{\text{classifications}}{\text{s}}$	$\frac{0.22\text{ pJ}}{\text{classification}}$	19
[17]	RBF	86.90%	90.12%	92.90%	$29.43\mu W$	$200k\frac{\text{classifications}}{\text{s}}$	$\frac{147.15\text{ pJ}}{\text{classification}}$	12
[18]	MLP	94.70%	97.48%	99.70%	$434.32\mu W$	$930k\frac{\text{classifications}}{\text{s}}$	$\frac{466.97\text{ pJ}}{\text{classification}}$	19
[19]	LSTM	97.30%	99.12%	100.00%	$31.21mW$	$870M\frac{\text{classifications}}{\text{s}}$	$\frac{35.87\text{ pJ}}{\text{classification}}$	19
[20]	K-means	91.90%	95.87%	97.70%	$138.42\mu W$	$5M\frac{\text{classifications}}{\text{s}}$	$\frac{27.68\text{ pJ}}{\text{classification}}$	19
[21]	Fuzzy	88.30%	93.55%	97.30%	$2.49\mu W$	$4.55K\frac{\text{classifications}}{\text{s}}$	$\frac{547.2\text{ pJ}}{\text{classification}}$	12
[22]	GMM	87.30%	90.44%	93.40%	$3.14\mu W$	$100K\frac{\text{classifications}}{\text{s}}$	$\frac{31.4\text{ pJ}}{\text{classification}}$	12
[13]	Bayes	83.90%	88.33%	91.90%	$1.94\mu W$	$100K\frac{\text{classifications}}{\text{s}}$	$\frac{19.4\text{ pJ}}{\text{classification}}$	12
[23]	Threshold	88.30%	89.21%	93.10%	$1.09\mu W$	$100K\frac{\text{classifications}}{\text{s}}$	$\frac{10.9\text{ pJ}}{\text{classification}}$	12
[24]	SVM	89.90%	90.21%	91.20%	$73.28\mu W$	$140K\frac{\text{classifications}}{\text{s}}$	$\frac{523.43\text{ pJ}}{\text{classification}}$	12
[25]	Centroid	91.20%	93.28%	96.70%	$3.18\mu W$	$100K\frac{\text{classifications}}{\text{s}}$	$\frac{31.8\text{ pJ}}{\text{classification}}$	12

REFERENCES

[1] G. Rong, A. Mendez, E. B. Assi, B. Zhao, and M. Sawan, "Artificial intelligence in healthcare: review and prediction case studies," *Engineering*, vol. 6, no. 3, pp. 291–301, 2020.

[2] H. B. Mamo, M. Adamiak, and A. Kunwar, "3d printed biomedical devices and their applications: A review on state-of-the-art technologies, existing challenges, and future perspectives," *Journal of the Mechanical Behavior of Biomedical Materials*, p. 105930, 2023.

[3] E. M. Davidson, M. T. Poon, A. Casey, A. Grivas, D. Duma, H. Dong, V. Suárez-Paniagua, C. Grover, R. Tobin, H. Whalley *et al.*, "The reporting quality of natural language processing studies: systematic review of studies of radiology reports," *BMC medical imaging*, vol. 21, no. 1, pp. 1–13, 2021.

[4] A. Abernethy, L. Adams, M. Barrett, C. Bechtel, P. Brennan, A. Butte, J. Faulkner, E. Fontaine, S. Friedhoff, J. Halamka *et al.*, "The promise of digital health: Then, now, and the future," *NAM perspectives*, vol. 2022, 2022.

[5] K. Aboumerhi, A. Güemes, H. Liu, F. Tenore, and R. Etienne-Cummings, "Neuromorphic applications in medicine," *Journal of Neural Engineering*, vol. 20, no. 4, p. 041004, 2023.

[6] W. Haensch, T. Gokmen, and R. Puri, "The next generation of deep learning hardware: Analog computing," *Proceedings of the IEEE*, vol. 107, no. 1, pp. 108–122, 2018.

[7] B. J. MacLennan, "A review of analog computing," *Department of Electrical Engineering & Computer Science, University of Tennessee, Technical Report UT-CS-07-601 (September)*, 2007.

[8] C. Bachmann, M. Ashouei, V. Pop, M. Vidojkovic, H. De Groot, and B. Gyselinckx, "Low-power wireless sensor nodes for ubiquitous long-term biomedical signal monitoring," *IEEE Communications Magazine*, vol. 50, no. 1, pp. 20–27, 2012.

[9] M. U. Anjum, A. Fida, I. Ahmad, and A. Iftikhar, "A broadband electromagnetic type energy harvester for smart sensor devices in biomedical applications," *Sensors and Actuators A: Physical*, vol. 277, pp. 52–59, 2018.

[10] [Online]. Available: https://archive.ics.uci.edu/dataset/46/hepatitis

[11] C. M. Bishop and N. M. Nasrabadi, *Pattern recognition and machine learning*. Springer, 2006, vol. 4, no. 4.

[12] D. Castaneda, A. J. Gonzalez, M. Alomari, K. Tandon, and X. B. Zervos, "From hepatitis a to e: A critical review of viral hepatitis," *World journal of gastroenterology*, vol. 27, no. 16, p. 1691, 2021.

[13] V. Alimisis, G. Gennis, C. Dimas, and P. P. Sotiriadis, "An analog bayesian classifier implementation, for thyroid disease detection, based on a low-power, current-mode gaussian function circuit," in *2021 International conference on microelectronics (ICM)*. IEEE, 2021, pp. 153–156.

[14] P. Bertsias, C. Psychalinos, A. G. Radwan, and A. S. Elwakil, "High-frequency capacitorless fractional-order cpe and fi emulator," *Circuits, Systems, and Signal Processing*, vol. 37, no. 7, pp. 2694–2713, 2018.

[15] J. Lazzaro, S. Ryckebusch, M. A. Mahowald, and C. A. Mead, "Winner-take-all networks of o (n) complexity," *Advances in neural information processing systems*, vol. 1, 1988.

[16] S. T. Chandrasekaran, R. Hua, I. Banerjee, and A. Sanyal, "A fully-integrated analog machine learning classifier for breast cancer classification," *Electronics*, vol. 9, no. 3, p. 515, 2020.

[17] S.-Y. Peng, P. E. Hasler, and D. V. Anderson, "An analog programmable multidimensional radial basis function based classifier," *IEEE Transactions on Circuits and Systems I: Regular Papers*, vol. 54, no. 10, pp. 2148–2158, 2007.

[18] K. Lee, J. Park, and H.-J. Yoo, "A low-power, mixed-mode neural network classifier for robust scene classification," *Journal of Semiconductor Technology and Science*, vol. 19, no. 1, pp. 129–136, 2019.

[19] Z. Zhao, A. Srivastava, L. Peng, and Q. Chen, "Long short-term memory network design for analog computing," *ACM Journal on Emerging Technologies in Computing Systems (JETC)*, vol. 15, no. 1, pp. 1–27, 2019.

[20] R. Zhang and T. Shibata, "An analog on-line-learning k-means processor employing fully parallel self-converging circuitry," *Analog Integrated Circuits and Signal Processing*, vol. 75, pp. 267–277, 2013.

[21] E. Georgakilas, V. Alimisis, G. Gennis, C. Aletraris, C. Dimas, and P. P. Sotiriadis, "An ultra-low power fully-programmable analog general purpose type-2 fuzzy inference system," *AEU-International Journal of Electronics and Communications*, vol. 170, p. 154824, 2023.

[22] V. Alimisis, G. Gennis, K. Touloupas, C. Dimas, M. Gourdouparis, and P. P. Sotiriadis, "Gaussian mixture model classifier analog integrated low-power implementation with applications in fault management detection," *Microelectronics Journal*, vol. 126, p. 105510, 2022.

[23] V. Alimisis, G. Gennis, E. Tsouvalas, C. Dimas, and P. P. Sotiriadis, "An analog, low-power threshold classifier tested on a bank note authentication dataset," in *2022 International Conference on Microelectronics (ICM)*. IEEE, 2022, pp. 66–69.

[24] V. Alimisis, G. Gennis, M. Gourdouparis, C. Dimas, and P. P. Sotiriadis, "A low-power analog integrated implementation of the support vector machine algorithm with on-chip learning tested on a bearing fault application," *Sensors*, vol. 23, no. 8, p. 3978, 2023.

[25] V. Alimisis, V. Mouzakis, G. Gennis, E. Tsouvalas, C. Dimas, and P. P. Sotiriadis, "A hand gesture recognition circuit utilizing an analog voting classifier," *Electronics*, vol. 11, no. 23, p. 3915, 2022.